TU Delft

Delft University of Technology

Pulsed-field array performance

A TD analysis

Lager, Ion E.

DOI
10.1109/EuRAD.2015.7346335

Publication date
2015

Document Version
Accepted author manuscript

Published in
Proceedings of the 12th European Radar Conference, EuRAD 2015

Citation (APA)
Lager, I. E. (2015). Pulsed-field array performance: A TD analysis. In H. Aubert, L. Ferro-Famil, J. M. Goutoule, & M. Lalande (Eds.), *Proceedings of the 12th European Radar Conference, EuRAD 2015* (pp. 453-456). IEEE. https://doi.org/10.1109/EuRAD.2015.7346335

Important note
To cite this publication, please use the final published version (if applicable).
Please check the document version above.

Copyright
Other than for strictly personal use, it is not permitted to download, forward or distribute the text or part of it, without the consent of the author(s) and/or copyright holder(s), unless the work is under an open content license such as Creative Commons.

Takedown policy
Please contact us and provide details if you believe this document breaches copyrights.
We will remove access to the work immediately and investigate your claim.

This work is downloaded from Delft University of Technology.
For technical reasons the number of authors shown on this cover page is limited to a maximum of 10.

Pulsed-field array performance: A TD analysis

Ioan E. Lager
Delft University of Technology, Faculty of Electrical Engineering, Mathematics and Computer Science,
Mekelweg 4, 2628 CD Delft, the Netherlands
Email: i.e.lager@tudelft.nl

***Abstract*—The pulsed-field excited array antenna performance is studied via full time-domain instruments. The directional distribution of radiated energy and the directional (system) fidelity factor are employed as performance metrics. Illustrative numerical experiments highlight the expedient radiation features that are specific to pulse-train excited, linear array antennas. The analysis provides an expedient reference for estimating the detectability of the signals radiated by pulse-train excited array antennas, as needed in ultra-high rate wireless digital transfer.**

I. Introduction

Signal integrity is conditional for recovering the received binary values in wireless digital transfer [1]. Ensuring this feature in future ultra-high rate digital communication systems is carried out by means of increasingly sophisticated design procedures requiring, among others, an accurate characterisation of the received signals. In this respect, electromagnetic (EM) models can opportunely predict the system's performance under certain simple, but relevant conditions, thus providing expedient best-case estimators. Since [2] conjectured that digital signal transfer is best supported by *pulsed* electromagnetic (EM) field transfer, such models are most adequately built via time-domain (TD) instruments.

Wireless digital transfer requires transmitting and receiving *trains* of *pulses*. All pulses in EM models should then have analytical expressions characterised by generally accepted parameters [3], [4], and be sent at regular intervals, this inducing a pulse repetition rate. These pulse-trains undergo alterations during the transmitter $\rightarrow$ receiver transfer, and the wireless digital transfer's reliability hinges on minimising or, at least, accurately predicting these temporal alterations. Moreover, for increasing the energy of the received signals and, thus, improving their detection in background noise, wireless systems often resort to energy focusing by means of array antennas on the transmit and/or receive side. The element spreading also affects the received signatures via constructive/destructive interference caused by the different path lengths involved.

This work analyses the performance of transmitting pulsed-field array antennas. The directional distribution of radiated energy is evaluated by means of the instruments introduced in [5]. The quality of the radiated field signatures is studied via the *system's fidelity factor* [6], its scope being extended as *directional signal fidelity factor* for also accounting for the array antenna's beam-steering properties. In [7] this metric was restricted to a subsystem of the transmission chain, namely the array configuration. However, in this study preference is given to a full-system interpretation of the fidelity factor (as defined in, e.g., [8]) with the reference signal being taken as the electric current injected at the Kirchhoff port of the reference element of the array. Like in [7], the hereby employed directional signal fidelity factor is a purely directional quantity.

This account proceeds by succinctly reiterating some of the main results in [5], [7], with some technicalities being presented in the appendix. Illustrative numerical experiments concerning (non-)uniform, linear arrays will then be elaborately discussed. The account will end with conclusions.

II. Radiation of array antennas composed of pulsed electric-current excited elements

A. Examined configuration

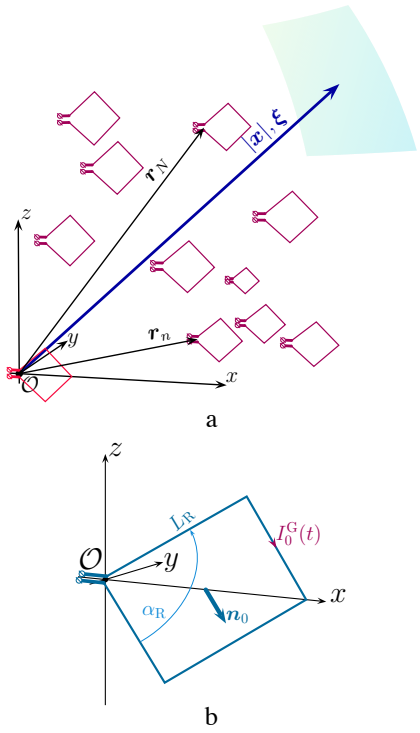

Fig. 1. Investigated configuration. (a) Antenna array composed of identical, translationally shifted elements; (b) rhombic antenna (reference) element; its geometric parameters are the opening angle $\alpha_{\rm R}$ and the side length $L_{\rm R}$; two element orientations are considered: either $\boldsymbol{n}_0\cdot\boldsymbol{i}_z=0$ or $\boldsymbol{n}_0\cdot\boldsymbol{i}_z=1$.

The array antenna consists of $N+1$, $N=0,1,2\ldots$, identical, mutually translationally shifted, pulsed electric-current excited elements (Fig. 1.a). Position in the configuration is specified by the position vector $\boldsymbol{x}\in\mathbb{R}^3$. The time coordinate is $t\in\mathbb{R}$. The elments' reference points are $\boldsymbol{r}_n$, $n=1,\ldots,N$. The array radiates into free space, with electric permittivity ε_0, magnetic permeability μ_0 and corresponding wavespeed $c_0=(\varepsilon_0\mu_0)^{-½}$. The array is taken to consist of rhombic wire antennas, the considered (reference) element being shown in Fig. 1.b. The elements' Kirchhoff circuit ports are excited with electric currents $I_n^{\rm G}(t)$. More configurational details are given in [5], [7].

B. The radiated field

As demonstrated in [5], [7], the TD radiated EM field is expressed in the far-field region [9, pp. 762–768] as

$$\{\boldsymbol{A},\boldsymbol{E},\boldsymbol{H}\}(\boldsymbol{x},t) = \frac{\{\boldsymbol{A}^{\infty},\boldsymbol{E}^{\infty},\boldsymbol{H}^{\infty}\}(\boldsymbol{\xi},t-|\boldsymbol{x}|c_0^{-1})}{4\pi|\boldsymbol{x}|}\left[1+O(|\boldsymbol{x}|^{-1})\right] \quad \text{as } |\boldsymbol{x}|\to\infty \tag{1}$$

with $\mathcal{O}$ as the reference center and $\boldsymbol{\xi}=\boldsymbol{x}/|\boldsymbol{x}|$ as the unit vector in the direction of observation. Here, $\{\boldsymbol{A},\boldsymbol{E},\boldsymbol{H}\}(\boldsymbol{x},t)$ are the electric-current potential, and the electric and the magnetic field strengths, respectively, their corresponding far-field radiation characteristics $\{\boldsymbol{A}^{\infty},\boldsymbol{E}^{\infty},\boldsymbol{H}^{\infty}\}(\boldsymbol{\xi},t)$ being interrelated by [9, Eqs. (26.3-13) and (26.3-16)]

$$\boldsymbol{E}^{\infty} = -\mu_0[\partial_t\boldsymbol{A}^{\infty} - \boldsymbol{\xi}(\boldsymbol{\xi}\cdot\partial_t\boldsymbol{A}^{\infty})] \tag{2}$$

$$\boldsymbol{H}^{\infty} = -c_0^{-1}\boldsymbol{\xi}\times\partial_t\boldsymbol{A}^{\infty}. \tag{3}$$

For the considered array, $\boldsymbol{A}^{\infty}$ is obtained by superposition

$$\boldsymbol{A}^{\infty} = \sum_{n=0}^{N}\boldsymbol{A}_n^{\infty}, \tag{4}$$

with $\boldsymbol{A}_n^{\infty}$ following via time convolutions of $I_n^{\mathrm{G}}(t)=I_0^{\mathrm{G}}(t-T_n)$ ($T_n=$ time delays) and configurational quantities. Constructive interference of the element contributions occurs if

$$T_n = c_0^{-1}\boldsymbol{\xi}_{\mathrm{st}}\cdot\boldsymbol{r}_n, \ \text{ for } n=1,2,3,\ldots,N \tag{5}$$

the resulting $\boldsymbol{\xi}_{\mathrm{st}}$ specifying the direction of the main beam ('direction of steering').

C. Array performance metrics

1) The area density of radiated energy: The energy W^{rad} radiated by the array is expressed as

$$W^{\mathrm{rad}} = \int_{\boldsymbol{\xi}\cdot\boldsymbol{\xi}=1}\boldsymbol{\Phi}^{\mathrm{rad}}(\boldsymbol{\xi})\cdot\boldsymbol{\xi}\,\mathrm{d}\Omega, \tag{6}$$

in which $\boldsymbol{\Phi}^{\mathrm{rad}}(\boldsymbol{\xi})$ is the area density of radiated energy in the direction $\boldsymbol{\xi}$. For free space radiation, it is found that [5]

$$\boldsymbol{\Phi}^{\mathrm{rad}}(\boldsymbol{\xi}) = \frac{Z_0}{16\pi^2\,c_0^2}\,\boldsymbol{\xi}\int_{t\in\mathbb{R}}\left[\partial_t\left(\boldsymbol{\xi}\times\boldsymbol{A}^{\infty}\right)\cdot\partial_t\left(\boldsymbol{\xi}\times\boldsymbol{A}^{\infty}\right)\right]\mathrm{d}t \tag{7}$$

with $Z_0=(\mu_0/\varepsilon_0)^{1/2}$ denoting the free space electromagnetic wave impedance. The area density of radiated energy is examined via polar diagrams of the normalised area density of radiated energy

$$D_{\mathrm{dB}}(\boldsymbol{\xi}) = 10\log_{10}\left[\boldsymbol{\Phi}^{\mathrm{rad}}(\boldsymbol{\xi})\cdot\boldsymbol{\xi}/4\pi W^{\mathrm{rad}}\right]. \tag{8}$$

2) The directional signal fidelity factor: The analysis of the system's fidelity factor starts from the expression [8]

$$F(S_{\mathrm{sys}},S_{\mathrm{ref}}) = \max_{\tau}\int_{t=-\infty}^{\infty}\frac{S_{\mathrm{sys}}(t)}{\|S_{\mathrm{sys}}(t)\|}\frac{S_{\mathrm{ref}}(t-\tau)}{\|S_{\mathrm{ref}}(t)\|}\mathrm{d}t \tag{9}$$

in which S_{sys} and S_{ref} are *scalar* signals and the maximum of the normalised cross-correlation integral is obtained empirically. Henceforth, $S_{\mathrm{sys}}(t)$ is taken to be representative for the far-field EM radiation in the direction $\boldsymbol{\xi}$, namely $E_z^{\infty}(\boldsymbol{\xi})$ for array antennas with $\boldsymbol{n}_0\cdot\boldsymbol{i}_z=0$ type elements and $E_y^{\infty}(\boldsymbol{\xi})$ for those with $\boldsymbol{n}_0\cdot\boldsymbol{i}_z=1$ type elements (see Fig. 1.b). The reference signal $S_{\mathrm{ref}}(t)$ is taken as the second time derivative of the current injected at the Kirchhoff port of the reference element (see Appendix B). With these choices, the resulting signal fidelity factor is a purely directional quantity termed *directional signal fidelity factor*

$$F_{\mathrm{f}}(\boldsymbol{\xi}) = \max_{\tau}\int_{t=-\infty}^{\infty}\frac{E_{y,z}(\boldsymbol{\xi},t)}{\|E_{y,z}(\boldsymbol{\xi},t)\|}\frac{\partial_t^2 I_0^{\mathrm{G}}(t-\tau)}{\|\partial_t^2 I_0^{\mathrm{G}}(t)\|}\mathrm{d}t. \tag{10}$$

Only the positive $F_{\mathrm{f}}(\boldsymbol{\xi})$ are considered in this work, with negative cross-correlations yielding a zero fidelity factor. From a practical point of view, this choice assumes a receiving system capable of discriminating between a 'positive' and a 'negative' incoming signal, this offering additional spatial filtering capabilities. When such a discrimination is not possible, the absolute value of the numerator must be taken in (10).

III. Illustrative numerical experiments

The performance of pulse-train excited array antennas is now examined by using the metrics introduced in Section II-C.

A. Excitation electric current shapes

The shapes of the electric currents $I_n^{\mathrm{G}}(t)$ exciting the Kirchhoff circuit ports of the array elements are taken as short trains of monocycle (d_tPE) pulses. Their expression follows from the normalised power exponential (PE) pulse [3] of pulse rise time $t_{\mathrm{r}}>0$ and pulse rising power $\nu>1$ (with ν being confined to integer values in this study) as

$$\begin{aligned}\mathrm{d}_t\mathrm{PE}(t) &= t_{\mathrm{r}}N(\nu)\,\partial_t\mathrm{PE}(t)\\ &= N(\nu)\left(t'^{\nu-1}-t'^{\nu}\right)\exp\left[-\nu\left(t'-1\right)\right]H(t)\end{aligned} \tag{11}$$

where $t'=t/t_{\mathrm{r}}$, $N(\nu)=\nu^{-1/2}\left[\nu^{1/2}/(\nu^{1/2}-1)\right]^{\nu-1}\exp(-\nu^{1/2})$ ensures a unit amplitude for d_tPE and $H(\cdot)$ is the Heaviside unit step function. The electric current injected at the Kirchhoff port of the reference element in the array is then taken as

$$I_0^{\mathrm{G}}(t) = \sum_{m=0}^{M} I_0\ \mathrm{d}_t\mathrm{PE}(t+mR_{\mathrm{r}}) \tag{12}$$

with I_0 being the electric current amplitude and R_{r} the pulse repetition rate. The current excitations of the remaining elements are time delayed according to (5).

The expressions of the EM field quantities in Section II-B were established in [5], [7] based on a quasi-static regime operation assumption. To enforce this, the side lengths are taken as $L_{\mathrm{R}}=c_0t_{\mathrm{w}}/20$, with the pulse time width t_{w} being derived in line with [3, Eq. (23)] as

$$t_{\mathrm{w}} = \int_0^{t_{\mathrm{r}}}\mathrm{d}_t\mathrm{PE}(t)\mathrm{d}t = t_{\mathrm{r}}N(\nu)\int_0^{t_{\mathrm{r}}}\partial_t\mathrm{PE}(t)\mathrm{d}t = t_{\mathrm{r}}N(\nu). \tag{13}$$

B. Single element experiments

The case of isolated rhombic antennas is firstly investigated. The directional diagrams, not included in this paper for brevity, evidence the 'doughnut' shaped $D_{\mathrm{dB}}(\boldsymbol{\xi})$ pattern that is characteristic for dipoles, with the nulls in the direction perpendicular to the rhomb's plane, and a $F_{\mathrm{f}}(\boldsymbol{\xi})$ that is approximately one in all directions, except in the ones corresponding to the radiation nulls.

C. Uniform linear array experiments

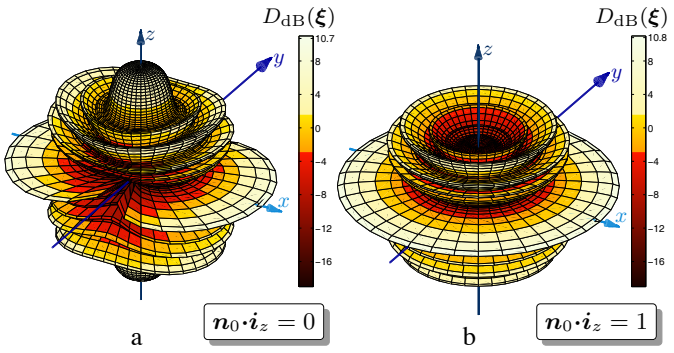

Fig. 2. $D_{\rm dB}(\boldsymbol{\xi})$ pattern for a uniform, linear array consisting of 8 rhombic antennas; excitation: a train of 5 d_tPE pulses with a $R_{\rm r}$ pulse repetition rate; inter-element spacing: $c_0 R_{\rm r}/2$; broadside beam steering.

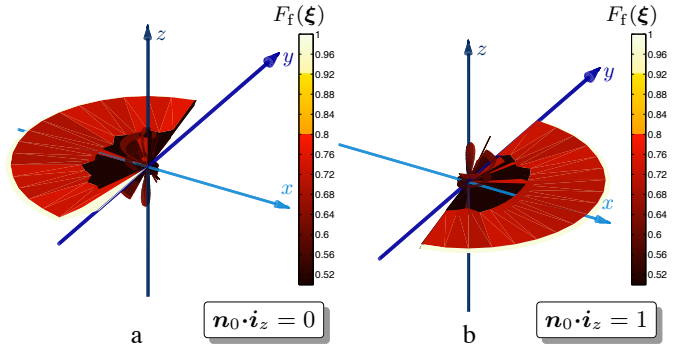

Fig. 3. Fidelity factor pattern for the array examined in Fig. 2.

The case of uniform linear array antennas consisting of 8 elements is now studied. The elements are located at $\boldsymbol{r}_n = z_n^{\rm U}\boldsymbol{i}_z$, in which $z_n^{\rm U} = n\,(\mathcal{K} c_0 R_{\rm r}/2)$, $n = 0, 1, 2, \ldots, 7$, and $\mathcal{K} \geqslant 1$ is a scaling factor. $D_{\rm dB}(\boldsymbol{\xi})$ patterns are given in Fig. 2 for broadside beam steering and $\mathcal{K} = 1$ (see [7] for beam scanning experiments). The main beam is clearly visible. The largest sidelobes correspond to constructive interference of delayed elementary contributions from *a part* of the array elements, as also observed in [10]. There are, also, sidelobes that are not related to correspondences between the pulse repetition rate and element locations, such as those pointing in the $\boldsymbol{i}_z$ – direction in Fig. 2.a. Such lobes have also been observed in the patterns reported in [5] for single-pulse excitations.

The $F_{\rm f}(\boldsymbol{\xi})$ patters are shown in Fig. 3. These plots evidence that the fidelity factor is, practically, one in the main beam and drops rapidly outside it. Moreover, $F_{\rm f}(\boldsymbol{\xi}) = 0$ in the half-space where, due to field symmetry, the radiated field has opposite direction. It can then be inferred that accounting for the signal's fidelity increases the spatial selectivity offered by the array's focusing (with an additional gain of about 3dB). This is important for ultra-high rate digital transfer, from both effectiveness and communication security points of view.

D. Non-uniform linear array experiments

The last study concerns non-uniform, linear array antennas synthesised according to the placement strategy in [11]. Firstly, for consistency with the uniform linear array experiment, an arrays consisting of 8 elements and having the same length is considered. Its elements are placed at $\boldsymbol{r}_n = z_n^{\rm CDS}\boldsymbol{i}_z$, in which

$$z_n^{\rm CDS} = \{0, 10, 12, 13, 18, 27, 34, 38\}/38 \;\; (7\, c_0 R_{\rm r}/2) \quad (14)$$

follow from the by 12 shifted, modulo 57, cyclic permutation of the $\{57, 8, 1\}$ Cyclic Difference Set (CDS) [12]. The broadside $D_{\rm dB}(\boldsymbol{\xi})$ patterns are given in Fig. 4. These plots evidence a remarkable difference with respect to those in Fig. 2, namely the practical absence of (high) sidelobes – a feature following from the two-valued autocorrelation property of CDS's at the core of the design strategy in [11]. The $F_{\rm f}(\boldsymbol{\xi})$ patterns (see Fig. 5) preserve the main features of those in Fig. 3. There is a slight fidelity factor increase of $F_{\rm f}(\boldsymbol{\xi})$ in the sidelobes, this diminishing the combined directivity↔fidelity gain.

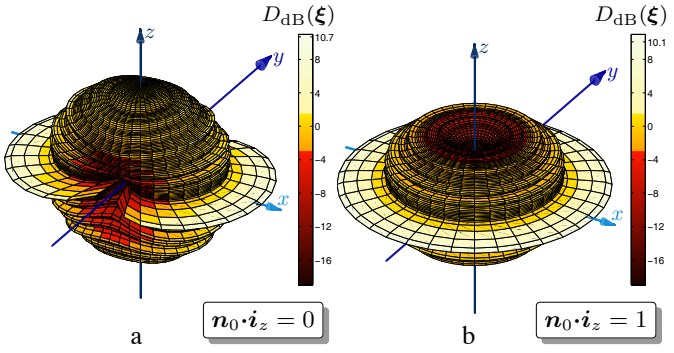

Fig. 4. $D_{\rm dB}(\boldsymbol{\xi})$ pattern for a linear array consisting of 8 rhombic antennas; excitation: a train of 5 d_tPE pulses with a $R_{\rm r}$ pulse repetition rate; CDS placement yielding a $7\, c_0 R_{\rm r}/2$ array length; broadside beam steering.

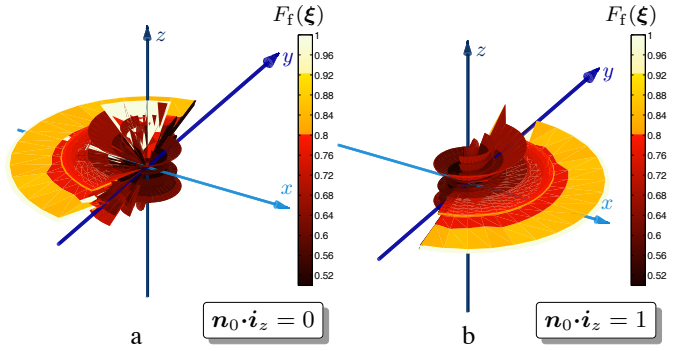

Fig. 5. Fidelity factor pattern for the array examined in Fig. 4.

Finally, the performance of a similarly CDS-synthesised linear array with a total length of $70\, c_0 R_{\rm r}/2$ is examined. Despite the huge interelement spacing, no high sidelobes are present in the $D_{\rm dB}(\boldsymbol{\xi})$ patern (Fig. 6). This unique feature, a direct consequence of the conjunction between the two-valued autocorrelation of the element locations and the pulse-train finiteness, renders pulsed-field array antennas superior to time-harmonic arrays in which case the high sidelobes (actually, grating lobes) free operation is only obtained up to a maximum inter-element spacing. The $F_{\rm f}(\boldsymbol{\xi})$ pattern (Fig. 7) is also extremely opportune.

IV. Conclusions

The performance of pulsed-field excited array antennas was studied via full time-domain instruments. The directional distribution of radiated energy and the directional (system)

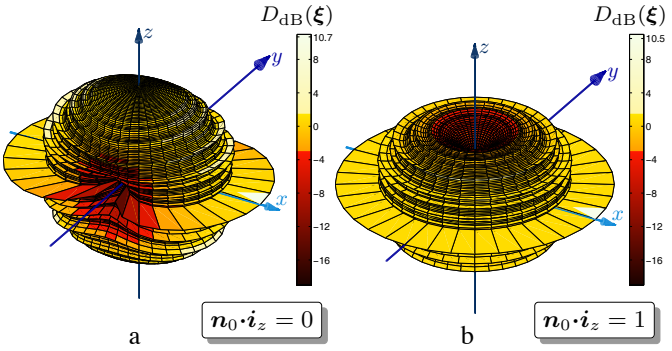

Fig. 6. $D_{\mathrm{dB}}(\boldsymbol{\xi})$ pattern for a linear array consisting of 8 rhombic antennas; excitation: a train of 5 d_tPE pulses with a R_{r} pulse repetition rate; CDS placement yielding a $70\,c_0R_{\mathrm{r}}/2$ array length; broadside beam steering.

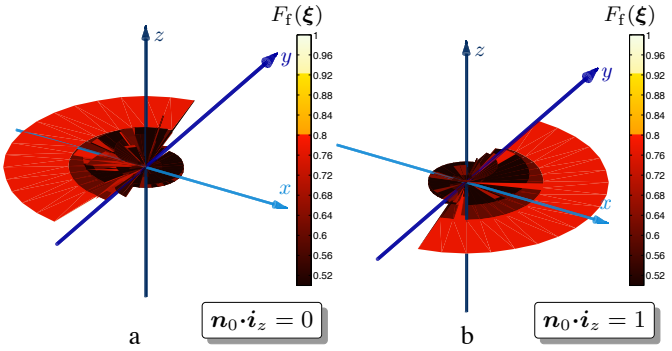

Fig. 7. Fidelity factor pattern for the array examined in Fig. 6.

fidelity factor were employed as expedient performance metrics. The study demonstrated that accounting for the signal's fidelity improves the spatial selectivity offered by the arrays' intrinsic focusing properties, with up to 3dB additional gain being achievable. The analysis of non-uniform, linear array antennas with extreme lengths has demonstrated their ability to generate narrow beams without the onset of high sidelobes. The highlighted performance is expedient, via energy focusing, for enhancing the detectability of signals in background noise and, via increased spatial selectivity, for improved communication security, making pulsed-field excited array antennas highly opportune for ultra-high rate wireless digital transfer.

APPENDIX

A. The TD field radiated by array antennas consisting of rhombic elements

For evaluating the EM field radiated by the array antennas considered in this paper, it is observed that $\boldsymbol{A}_n^{\infty}$ in (4) correspond to fields radiated by straight wire segments of length L_{R}. Let such a segment be oriented from the point with position vector $\boldsymbol{x}_{\mathcal{P}}$ to the point with position vector $\boldsymbol{x}_{\mathcal{Q}}$, let $\boldsymbol{\tau}_{\mathcal{PQ}}=(\boldsymbol{x}_{\mathcal{Q}}-\boldsymbol{x}_{\mathcal{P}})/L_{\mathrm{R}}$, and let $I_n(t)$ be the electric current carried by it. The $\boldsymbol{A}_n^{\infty}$ is then expressed as [5]

$$\partial_t\boldsymbol{A}_{n,\perp}^{\infty}(\boldsymbol{\xi},t)=(\boldsymbol{\tau}_{\mathcal{PQ}}L_{\mathrm{R}})\,\partial_t I_n(t+T_{\mathcal{P}}) \tag{15}$$

in case $\boldsymbol{\xi}\cdot\boldsymbol{\tau}_{\mathcal{PQ}}=0$ or as

$$\partial_t\boldsymbol{A}_{n,\not\perp}^{\infty}(\boldsymbol{\xi},t)=(\boldsymbol{\tau}_{\mathcal{PQ}}L_{\mathrm{R}})\,\frac{I_n\,(t+T_{\mathcal{Q}})-I_n\,(t+T_{\mathcal{P}})}{(\boldsymbol{\xi}\cdot\boldsymbol{\tau}_{\mathcal{PQ}})\,c_0^{-1}L_{\mathrm{R}}} \tag{16}$$

in case $\boldsymbol{\xi}\cdot\boldsymbol{\tau}_{\mathcal{PQ}}\neq 0$, with $T_{\mathcal{P},\mathcal{Q}}=c_0^{-1}\boldsymbol{\xi}\cdot\boldsymbol{x}_{\mathcal{P},\mathcal{Q}}$. Note that for deriving (15) and (16) it was assumed that $I_n(t)$ has a linear spatial variation along the wire segment, this being consistent with the choice $L_{\mathrm{R}}\ll c_0t_{\mathrm{w}}$ (see Section II-A).

B. The reference signal for fidelity factor evaluation

To identify the reference signal $S_{\mathrm{ref}}(t)$ in (9), (16) is written as

$$\begin{aligned}\partial_t\boldsymbol{A}_{n,\not\perp}^{\infty}(\boldsymbol{\xi},t)&=\partial_t\boldsymbol{A}_{n,\perp}^{\infty}(\boldsymbol{\xi},t)\\&+(\boldsymbol{\tau}_{\mathcal{PQ}}L_{\mathrm{R}})\,\frac{(\boldsymbol{\xi}\cdot\boldsymbol{\tau}_{\mathcal{PQ}})\,c_0^{-1}L_{\mathrm{R}}}{2}\partial_t^2 I_n\,(t+T_{\mathcal{P}})\\&+(\boldsymbol{\tau}_{\mathcal{PQ}}L_{\mathrm{R}})\;O\big[(\boldsymbol{\xi}\cdot\boldsymbol{\tau}_{\mathcal{PQ}})\,c_0^{-1}L_{\mathrm{R}}\big]^3\end{aligned} \tag{17}$$

where use was made of the fact that $c_0^{-1}L_{\mathrm{R}}\ll t_{\mathrm{w}}$ and O is the Landau order notation [9, p. 1019]. Since the sides in each rhombic antenna form a closed contour, the terms $\partial_t\boldsymbol{A}_{n,\perp}^{\infty}(\boldsymbol{\xi},t)$ will cancel out. By now invoking the results in Section II-B, the thought for reference signal is then taken as the second order time derivative of the current injected at the Kirchhoff port of the reference element in the array, as given in (12).

ACKNOWLEDGMENT

The author expresses his entire gratitude to Professor Adrianus T. de Hoop for his conditional support in the derivation of this paper's theoretical background and for his conducing guidance in the TD performance analysis of array antennas.

REFERENCES

[1] J. F. Buckwalter, "Predicting microwave digital signal integrity," *IEEE Trans. Adv. Packag.*, vol. 32, no. 2, pp. 280–289, May 2009.

[2] I. E. Lager, R. B. Staszewski, A. B. Smolders, and D. M. W. Leenaerts, "Ultra-high data-rate wireless transfer in a saturated spectrum – new paradigms," in *Proc. 44^{th} EuMC*, 2014, pp. 917–920.

[3] I. E. Lager, A. T. de Hoop, and T. Kikkawa, "Model pulses for performance prediction of digital microlectronic systems," *IEEE Trans. Compon., Packag., Manuf. Technol.*, vol. 2, no. 11, pp. 1859–1870, Nov. 2012.

[4] I. E. Lager and A. T. de Hoop, "Causal pulses with rectangular spectral content: A tool for TD analysis of UWB antenna performance," *IEEE Antennas Wireless Propag. Lett.*, vol. 12, no. 1, pp. 1488–1491, Dec. 2013.

[5] I. E. Lager and A. T. de Hoop, "TD radiation properties of array antennas composed of pulsed electric-current excited elements," *IEEE Antennas Wireless Propag. Lett.*, vol. 15, 2015.

[6] D. Lamensdorf and L. Susman, "Baseband-pulse-antenna techniques," *IEEE Antennas Propag. Mag.*, vol. 36, no. 1, pp. 20–30, Feb. 1994.

[7] A. T. de Hoop and I. E. Lager, "Signal Integrity in Pulse-train Excited Array Antennas in Time and Space – A Full TD Analysis," in *Proc. 9^{th} EuCAP*, 2015.

[8] E. Pancera, T. Zwick, and W. Wiesbeck, "Spherical fidelity patterns of UWB antennas," *IEEE Trans. Antennas Propag.*, vol. 59, no. 6, pp. 2111–2119, June 2011.

[9] A. T. de Hoop, *Handbook of Radiation and Scattering of Waves*, London: Academic Press, 1995, xxx + 1085 pp.; electronic reproduction (with corrections) 2008, freely downloadable, for private use, from http://www.atdehoop.com.

[10] A. Shlivinski, "Kinematic properties of short-pulsed sparse transmitting arrays," *Progress in Electromagnetics Research*, vol. 115, pp. 11–33, 2011, [Online]. doi:10.2528/PIER11020901.

[11] D. G. Leeper, "Isophoric arrays – massively thinned phased arrays with well-controlled sidelobes," *IEEE Trans. Antennas Propag.*, vol. 47, no. 12, pp. 1825–1835, Dec. 1999.

[12] D. Gordon, "La Jolla cyclic difference set repository". [Online]. Available: www.ccrwest.org/diffsets.html.